HHS Public Access

Author manuscript

Angew Chem Int Ed Engl. Author manuscript; available in PMC 2022 September 06.

Published in final edited form as:

Angew Chem Int Ed Engl. 2021 September 06; 60(37): 20325–20330. doi:10.1002/anie.202103228.

Electrochemical Modulation of Carbon Monoxide-Mediated Cell Signaling

Jimin Park[a],[b], **Joy S. Zeng**[c], **Atharva Sahasrabudhe**[b],[d], **Kyoungsuk Jin**[c], **Yoel Fink**[a], **Karthish Manthiram**[c], **Polina Anikeeva**[a],[b],[e]

[a]Department of Materials Science and Engineering, Massachusetts Institute of Technology, Cambridge, MA 02139, USA

[b]Research Laboratory of Electronics and McGovern Institute for Brain Research, Massachusetts Institute of Technology, Cambridge, MA 02139, USA

[c]Department of Chemical Engineering, Massachusetts Institute of Technology, Cambridge, MA 02139, USA

[d]Department of Chemistry, Massachusetts Institute of Technology, Cambridge, MA 02139, USA

[e]Department of Brain and Cognitive Sciences, Massachusetts Institute of Technology, Cambridge, MA 02139, USA

Abstract

Despite the critical role played by carbon monoxide (CO) in physiological and pathological signaling events, current approaches to deliver this messenger molecule are often accompanied by off-target effects and offer limited control over release kinetics. To address these challenges, we developed an electrochemical approach that affords on-demand release of CO through reduction of carbon dioxide (CO_2) dissolved in the extracellular space. Electrocatalytic generation of CO by cobalt phthalocyanine molecular catalysts modulates signaling pathways mediated by a CO receptor, soluble guanylyl cyclase. Furthermore, by tuning the applied voltage during electrocatalysis, we explore the effect of the CO release kinetics on CO-dependent neuronal signaling. Finally, we integrate components of our electrochemical platform into microscale fibers to produce CO in a spatially-restricted manner and to activate signaling cascades in the targeted cells. By offering on-demand local synthesis of CO, our approach may facilitate the studies of physiological processes affected by this gaseous molecular messenger.

Graphical Abstract

jiminp@mit.edu, karthish@mit.edu, anikeeva@mit.edu.

Supporting information for this article is given via a link at the end of the document.

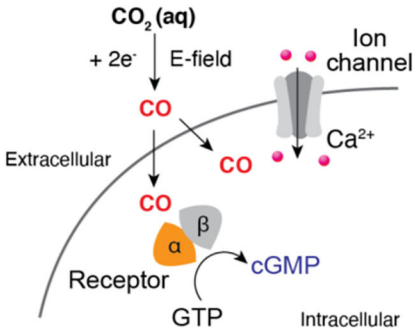

We devise an electrochemical strategy to locally synthesize carbon monoxide (CO), a gaseous messenger molecule, with tunable kinetics. By integrating this strategy with fiber-based fabrication, diverse CO-dependent signaling pathways in genetically engineered cells or neurons can be modulated at the microscale.

Keywords

carbon monoxide; cell signaling; electrochemistry; fiber drawing; receptors

Introduction

Carbon monoxide (CO) is a gaseous and transmembrane diffusible messenger affecting numerous physiological and pathological processes, including vasoactive response, neurotransmission, and inflammation[1–5]. To understand the physiological effects of CO and potentially harness them in a therapeutic context, prior work has explored direct delivery of CO gas via respiratory administration[2,6]. However, this approach does not permit targeting of CO to specific tissues or organs and poses a risk of a global increase in carboxyhemoglobin levels manifesting in CO poisoning[2,7–9]. Consequently, CO-releasing molecules (CORMs), which release CO as a free gas or transfer it to biological molecules, have been designed for targeted delivery of CO[10–12]. However, it remains challenging to tune CO-release kinetics of CORMs without modifying their molecular structures, and thus multiple CORMs are necessary for applications demanding variable CO release kinetics[2,11,13,14]. Moreover, degradation of inherently unstable CORMs during delivery limits precision of CO dosing often leading to off-target release beyond tissues of interest[7].

To circumvent these challenges, we developed a system that enables on-demand synthesis of CO through electrochemical CO_2 reduction reaction (Figure 1a). By leveraging a selective catalyst cobalt phthalocyanine (CoPc)[15–17], CO_2 dissolved in the extracellular solution can be reduced to CO at the cathode (Figure 1b). Due to its high solubility (~ 34 mM) in water, dissolved CO_2, which exists in equilibrium with bicarbonate buffer[16,18,19], serves as a precursor for electrochemical formation of CO. Electrochemically produced CO is shown to modulate diverse CO-dependent cell signaling processes *in vitro*. Furthermore, CO release kinetics can be controlled by varying the cathode voltage. This tunability of CO release kinetics enabled systematic investigation of neuronal signaling mediated by this molecule. Finally, we demonstrate microscale, CO-releasing electrocatalytic fibers as tools to locally activate cell signaling.

Results and Discussion

CoPc loaded cathodes were prepared by drop-casting CoPc ink (~ 1 mg/ml) onto the oxygen-functionalized carbon paper (OxCP). The electrocatalytic activities of CoPc/OxCP cathodes were evaluated in a three-compartment electrochemical cell containing physiological solution (Tyrode's) saturated with CO_2 at pH 7.4. Pt and Ag/AgCl electrodes were employed as anode and reference electrodes, respectively (Figure 1a, b). Cyclic voltammetry (CV) profiles of CoPc/OxCP in CO_2-saturated Tyrode's solution showed higher reductive currents as compared with those recorded in N_2-saturated solution (Figure 1c).

The cathodic products in CO_2-saturated Tyrode's solution were analyzed by chronoamperometry across a range of applied voltages. The cathodes exhibited high selectivity toward CO up to −1.3 V versus standard hydrogen electrode (SHE), and partial current density of CO increased as we applied more reductive potentials to the cathodes at this voltage range. Negligible amounts of H_2, a side product at the cathodes[15], were generated at identical reaction conditions with the Faradaic Efficiencies (FE) in the range of 1.8–3.4 % (Figure 1d). At higher negative voltages (≤ −1.5 V), hydrogen evolution reaction dominated over CO_2 reduction reaction (Figure 1d and Figure S1). At Pt anodes, oxygen evolution was predominately found with a minor chlorine evolution (Figure S2). Together, these data indicated that CO can be electrochemically generated from CO_2 dissolved in Tyrode's solution with high selectivity, and CO release kinetics can be controlled via applied voltage.

To illustrate the utility of our electrochemical system for modulating CO-dependent signaling, we first applied it to activate soluble guanylyl cyclase (sGC), one of the well-characterized receptors of CO[1–3]. It was previously shown that CO can bind to the heme moiety in sGC, activating the catalytic conversion of guanosine 5' triphosphate (GTP) to the second messenger cyclic guanosine 3',5'-monophosphate (cGMP)[20–22]. To elicit robustly measurable cGMP formation, human embryonic kidney (HEK) 293 FT cells were co-transfected with two plasmids carrying DDK-tagged α- and DDK-tagged β-subunits of human sGC under the broad mammalian cytomegalovirus (CMV) promoter, respectively. The expression of these subunits in the cells was confirmed by immunostaining with anti-DDK antibodies (Figure 2a). Consistent with previous reports[23,24], cells overexpressing both subunits (sGC^+ cells) exhibited substantially higher basal cGMP levels (~300 fold) as compared to unmodified cells only expressing low levels of endogenous sGC. In contrast, no noticeable increases in the cGMP levels were found after transfection of cells with either α-subunit or β-subunit alone (Figure 2b). When exposed to nitric oxide (NO), a highly potent activator of sGC[3,25], robust increase in cGMP levels (~20 fold) was found in sGC^+ cells, confirming the functionality of the genetically introduced sGC (Figure S3).

We next investigated whether electrochemically synthesized CO could activate sGC-cGMP signaling pathways (Figure 2c). We first confirmed that CoPc catalysts did not elicit any cytotoxic responses in HEK cells. Similarly, negligible cytotoxic responses were found in cells following acute exposure to CO_2-saturated Tyrode's solution (Figure S4). Additionally, we confirmed that the concentration of dissolved CO_2 at the bottom of the well plate,

where sGC^+ cells were located, remained largely constant over 30 min in the absence of continuous CO_2 purging (Figure S5). CO produced at the CoPc/OxCP cathodes at −1.3 V versus SHE in CO_2-saturated Tyrode's solution at pH 7.4 led to a moderate increase in cGMP levels (~150 %) in sGC^+ cells. To investigate whether the observed increase in cGMP is attributable to electrochemically formed CO, we recorded the cGMP levels in control groups, which included sGC^+ cells immersed in CO_2-saturated Tyrode's solution in the absence of an applied voltage and in the cells immersed in a solution not saturated in CO_2 in the presence of an applied voltage (−1.3 V versus SHE). Consistent with prior studies that found no changes in cGMP levels upon CO_2 delivery[26], no substantial increases in cGMP levels were observed in our control groups, indicating that electrochemically formed CO was responsible for sGC activation (Figure 2d).

Furthermore, electrochemically synthesized CO was sufficient to modulate the NO-mediated sGC-cGMP signaling in sGC^+ cells (Figure 2e). It has been previously proposed that CO, a weaker activator of sGC as compared to NO, could attenuate NO-mediated cGMP increases by competing for the same binding site (heme moiety of sGC) with NO[3,27]. Indeed, inhibitory effects of CO on NO-mediated sGC activation were found in a number of organs, including cerebellar cortex, retina, and resistance arteries[28–30]. Consistent with these prior studies[3,27], we observed noticeable decreases in NO-stimulated cGMP levels (~60 %) in sGC^+ cells following addition of 500 μM CORM-2 (tricarbonyldichlororuthenium(II) dimer), a molecular CO donor. Similarly, CO synthesized at CoPc/OxCP cathodes in CO_2-saturated Tyrode's solution led to attenuation in NO-mediated cGMP production (~70 %) (Figure 2f). These results suggested that the electrocatalytic CO-delivery approach could be extended to regulate diverse sGC-mediated signaling pathways.

We next evaluated whether our electrochemical system can be applied to interrogate CO-dependent signaling in neurons. Among the diversity of brain regions, hippocampus neurons have been shown to express high levels of heme oxygenase, which produces endogenous CO, implying that CO could play a critical role in hippocampal physiology[1,31]. Indeed, it has been reported that both endogenous and exogenous CO can trigger a myriad of processes in the hippocampus, including apoptosis, long-term potentiation, and expression of immediate early genes[32–34]. Thus we adopted hippocampal neurons as test beds for the CO-dependent signaling in neurons, and CO-triggered neuronal activity was recorded using an intracellular Ca^{2+} indicator fluo-4 as a proxy for neuronal membrane depolarization[35].

The effects of exogenous CO on hippocampal neurons were first investigated using CORM-2. When exposed to CORM-2 (50 μM), the normalized fluo-4 fluorescence ($\Delta F/F_0$) in hippocampal neurons gradually increased over time indicating Ca^{2+} influx into these cells, whereas the addition of an inactive form of CORM-2, $RuCl_3$, did not evoke any comparable fluorescence changes in neurons (Figure 3a, b). Addition of lower concentration of CORM-2 (from 1 to 10 μM) led to smaller Ca^{2+} influxes in neurons, indicating that observed Ca^{2+} signaling were predominantly triggered by CORM-2 (Figure 3c).

To investigate the biological mechanisms underlying the effects of CO-mediated Ca^{2+} influxes in neurons, we employed blockers (or inhibitors) of ion channels and receptors that have been previously proposed as molecular targets of CO[2,36–38]. The latter

included large-conductance, voltage- and Ca^{2+}-activated K^+-channel (BK_{Ca}), L-type Ca^{2+}-channel, hyperpolarization-activated cyclic nucleotide-gated channel (HCN), and sGC. Among blockers (or inhibitors) of the putative CO targets, L-type Ca^{2+} channel blocker nitrendipine[39] significantly attenuated Ca^{2+} responses driven by CORM-2 (Figure 3d and Figure S6). Although the understanding of the mechanisms contributing to the CO-mediated Ca^{2+} increases in neurons continues to evolve[36], our findings suggest that observed Ca^{2+} responses are at least partially related to the interactions between CO and L-type Ca^{2+} channels.

We then applied our electrochemical CO-delivery system to similarly evoke Ca^{2+} responses in hippocampal neurons (Figure 3e). Here, CoPc/OxCP cathode, Pt anode, and Ag/AgCl reference electrode were utilized to deliver CO to neurons in CO_2-saturated Tyrode's solution at pH 7.4. Because the local CO concentration is calculated to be much lower at greater distances from the cathode (Figure S5), we positioned the CoPc/OxCP cathode in the immediate vicinity of the neurons (Figure 3f). Robust Ca^{2+} responses (as marked by $\Delta F/F_0 \geq 25\%$) in neurons were observed 250 s after application of −1.3 V versus SHE, and continued application of −1.3 V to the cathode led to Ca^{2+} influxes in neurons located at greater distances from the cathode (Figure 3g, h). To assess whether observed Ca^{2+} responses were attributable to CO released from the cathodes, we recorded Ca^{2+} changes in control experiments, which included neurons immersed in CO_2-saturated Tyrode's solution with no voltage applied (Figure 3i) and in neurons immersed in Tyrode's not saturated in CO_2 in the presence of a cathodic bias (−1.3 V versus SHE, Figure 3j). The extent of Ca^{2+} responses found in the control experiments was significantly lower than that triggered by electrochemically formed CO (Figure 3h). Moreover, Ca^{2+} increases in response to CO released from the cathode were largely inhibited by the addition of L-type channel blocker nitrendipine (Figure S7), akin to our observations with CORM-2 (Figure 3d). These results suggested that Ca^{2+} responses observed in neurons are predominately mediated by electrochemically produced CO.

Our electrochemical approach further enabled an investigation of CO-mediated neuronal signaling at different CO release kinetics. When we applied −0.9 V versus SHE to the cathodes in CO_2-saturated Tyrode's solution, only 13% of neurons exhibited robust Ca^{2+} responses (as marked by $\Delta F/F_0 \geq 50\%$) (Figure 3k). In contrast, 91% of neurons responded at −1.3 V (Figure 3h) due to faster CO release kinetics at this voltage as compared to −0.9 V (Figure 1c, d). Despite the higher Faradaic current, a smaller fraction of neurons showed Ca^{2+} responses at −1.7 V as compared to −1.3 V (Figure 3l). This observation is consistent with the extremely low CO selectivity of CoPc/OxCP catalysts at this reductive voltage (Figure 1d and Figure S1). By controlling CO generation kinetics with applied voltage, we found that CO release kinetics, not Faradic current, is the key factor affecting CO-mediated Ca^{2+} responses in neurons.

Finally, we miniaturized our electrochemical system by leveraging fiber drawing[25,40]. Fiber-based fabrication allowed us to scale down macroscale components of an electrochemical cell into a microscopic electrocatalytic fiber (Figure 4a–d). A polycarbonate-based macroscopic preform, which contained two grooves on its surface for placing microelectrodes and one hollow channel for delivering CO_2-saturated solution, was

fabricated through macroscale machining (Figure 4b). During drawing, the preform was heated and stretched into a microscale fiber (Figure 4c, d). Carbon nanotube (CNT) and Pt microwires (50 μm in diameter) were then placed into grooves on the surface of the fiber. The microwires extended from the fiber tips by approximately 300 μm, and CoPc ink was deposited onto the CNT microwires. The non-exposed region of the microwires was then fully coated with epoxy that provided electrical insulation and mechanical stability, and the microwires and the microfluidic channel were interfaced with electrical pin connectors and tubing inlets, respectively (Figure 4e, f). We confirmed that CO_2-saturated Tyrode's solution can be delivered through the microfluidic channel integrated within the electrocatalytic fiber (Figure 4g). CoPc/CNT microwires, which served as cathodes integrated within the fibers, catalyzed CO_2 reduction reaction, as confirmed by chronoamperometry analyses (Figure 4h). Integrated Pt microwires served as anodes during the reaction.

The electrocatalytic fibers were then applied to locally deliver CO and evoke CO-mediated sGC-cGMP signaling cascades in the targeted cells. To monitor local cGMP dynamics, HEK cells were transfected with a plasmid carrying a genetically encoded fluorescent cGMP sensor, Green cGull[41], under the CMV promoter. The functionality of Green cGull expressed in cells was first confirmed with a NO releasing molecule (NORM) (Figure S8). After delivery of CO_2-saturated Tyrode's solution, CO was generated from the CoPc-CNT microwires at −1.3 V versus SHE. A gradual increase in Green cGull fluorescence (a marker of cGMP accumulation) was found in cells located in the proximity of the microwires (Figure 4i, j). In contrast, no noticeable Green cGull fluorescence changes were found in cells after delivery of CO_2-saturated solution in the absence of an applied voltage or in cells subjected to electric stimulation in the absence of CO_2 precursor (Figure 4j).

Conclusion

By leveraging electrocatalytic activity and selectivity of CoPc catalysts toward reduction of CO_2 into CO at modest voltages, we have developed an electrochemical approach for in situ targeted delivery of this molecule to physiological environments. Electrochemically released CO from CoPc-functionalized cathodes was shown to modulate several sGC-mediated signaling cascades in cells. Furthermore, facile control over CO release kinetics in our platform enabled a systematic investigation of CO-mediated signaling in neurons. This electrochemical system was further implemented in microscale fibers produced via thermal drawing. CO generated from the electrocatalytic fibers evoked local cGMP accumulation in the targeted cells. We envision that our electrochemical approach can be extended to explore CO-mediated cellular signaling in diverse systems, including the peripheral nervous system (Figure S9), offering addition insights onto its role as a messenger molecule.

Supplementary Material

Refer to Web version on PubMed Central for supplementary material.

Acknowledgements

We would like to thank T. Kitaguchi, and F. Zhang for the generous gifts of the plasmids and cell lines. The authors are also grateful to T. Khudiyev, S. Rao, and D. Rosenfeld for their technical advice on the experiments.

This work was funded in part by the National Institutes of Health (NIH) BRAIN Initiative (5-R01-MH111872, 1-R01-NS115576), the National Institute of Neurological Disorders and Stroke (1-R01-NS115025), the National Science Foundation (NSF) Center for Neurotechnology (EEC-1028725), the Hock E. Tan and K. Lisa Yang Center for Autism Research, and the McGovern Institute for Brain Research. Work by K.M. and J.S.Z. was supported by the NSF under grant no. 1955628. This work made use of the MIT MRSEC Shared Experimental Facilities under award number DMR-14-19807 from the NSF. J.P. is a recipient of scholarship from the Kwanjeong Educational Foundation. A.S. is a recipient of the Lore Harp McGovern graduate student fellowship.

References

[1]. Verma A, Hirsch DJ, Glatt CE, V Ronnett G, Snyder SH, Science (80-.)1993, 259, 381–384.

[2]. Motterlini R, Otterbein LE, Nat. Rev. Drug Discov2010, 9, 728. [PubMed: 20811383]

[3]. Ingi T, Cheng J, V Ronnett G, Neuron1996, 16, 835–842. [PubMed: 8608001]

[4]. Romão CC, Blättler WA, Seixas JD, Bernardes GJL, Chem. Soc. Rev2012, 41, 3571–3583. [PubMed: 22349541]

[5]. Otterbein LE, Bach FH, Alam J, Soares M, Tao Lu H, Wysk M, Davis RJ, Flavell RA, Choi AMK, Nat. Med2000, 6, 422–428. [PubMed: 10742149]

[6]. Allred EN, Bleecker ER, Chaitman BR, Dahms TE, Gottlieb SO, Hackney JD, Pagano M, Selvester RH, Walden SM, Warren J, Engl N. J. Med1989, 321, 1426–1432.

[7]. Meng J, Jin Z, Zhao P, Zhao B, Fan M, He Q, Sci. Adv2020, 6, DOI 10.1126/sciadv.aba1362.

[8]. Ernst A, Zibrak JD, Engl N. J. Med1998, 339, 1603–1608.

[9]. Heinemann SH, Hoshi T, Westerhausen M, Schiller A, Chem. Commun2014, 50, 3644–3660.

[10]. García-Gallego S, Bernardes GJL, Angew. Chemie Int. Ed2014, 53, 9712–9721.

[11]. Motterlini R, Clark JE, Foresti R, Sarathchandra P, Mann BE, Green CJ, Circ. Res2002, 90, e17–e24. [PubMed: 11834719]

[12]. Clark JE, Naughton P, Shurey S, Green CJ, Johnson TR, Mann BE, Foresti R, Motterlini R, Circ. Res2003, 93, e2–e8. [PubMed: 12842916]

[13]. Motterlini R, Sawle P, Bains S, Hammad J, Alberto R, Foresti R, Green CJ, FASEB J. 2005, 19, 1–24. [PubMed: 15629889]

[14]. Foresti R, Hammad J, Clark JE, Johnson TR, Mann BE, Friebe A, Green CJ, Motterlini R, Br. J. Pharmacol2004, 142, 453–460. [PubMed: 15148243]

[15]. Zhang X, Wu Z, Zhang X, Li L, Li Y, Xu H, Li X, Yu X, Zhang Z, Liang Y, Wang H, Nat. Commun2017, 8, 14675. [PubMed: 28272403]

[16]. Zeng JS, Corbin N, Williams K, Manthiram K, ACS Catal. 2020, 10, 4326–4336.

[17]. Zhu M, Ye R, Jin K, Lazouski N, Manthiram K, ACS Energy Lett. 2018, 3, 1381–1386.

[18]. Dunwell M, Lu Q, Heyes JM, Rosen J, Chen JG, Yan Y, Jiao F, Xu B, J. Am. Chem. Soc2017, 139, 3774–3783. [PubMed: 28211683]

[19]. Wuttig A, Yoon Y, Ryu J, Surendranath Y, J. Am. Chem. Soc2017, 139, 17109–17113. [PubMed: 28978199]

[20]. Ingi T, Chiang G, Ronnett GV, J. Neurosci1996, 16, 5621–5628. [PubMed: 8795618]

[21]. Zakhary R, Poss KD, Jaffrey SR, Ferris CD, Tonegawa S, Snyder SH, Proc. Natl. Acad. Sci1997, 94, 14848–14853. [PubMed: 9405702]

[22]. Kharitonov VG, Sharma VS, Pilz RB, Magde D, Koesling D, Proc. Natl. Acad. Sci1995, 92, 2568–2571. [PubMed: 7708686]

[23]. Parkinson SJ, Jovanovic A, Jovanovic S, Wagner F, Terzic A, Waldman SA, Biochemistry1999, 38, 6441–6448. [PubMed: 10350462]

[24]. Buechler WA, Nakane M, Murad F, Biochem. Biophys. Res. Commun1991, 174, 351–357. [PubMed: 1671207]

[25]. Park J, Jin K, Sahasrabudhe A, Chiang P-H, Maalouf JH, Koehler F, Rosenfeld D, Rao S, Tanaka T, Khudiyev T, Schiffer ZJ, Fink Y, Yizhar O, Manthiram K, Anikeeva P, Nat. Nanotechnol2020, 15, 690–697. [PubMed: 32601446]

[26]. YOU JP, WANG Q, ZHANG W, JANSEN-OLESEN I, PAULSON OB, LASSEN NA, EDVINSSON L, Acta Physiol. Scand1994, 152, 391–397. [PubMed: 7535505]

[27]. Marazioti A, Bucci M, Coletta C, Vellecco V, Baskaran P, Szabó C, Cirino G, Marques AR, Guerreiro B, Gonçalves AML, Seixas JD, Beuve A, Romão CC, Papapetropoulos A, Arterioscler. Thromb. Vasc. Biol2011, 31, 2570–2576. [PubMed: 21836072]

[28]. Kajimura M, Fukuda R, Bateman RM, Yamamoto T, Suematsu M, Antioxid. Redox Signal2010, 13, 157–192. [PubMed: 19939208]

[29]. Kajimura M, Shimoyama M, Tsuyama S, Suzuki T, Kozaki S, Takenaka S, Tsubota K, Oguchi Y, Suematsu M, FASEB J. 2003, 17, 1–23. [PubMed: 12522106]

[30]. Thorup C, Jones CL, Gross SS, Moore LC, Goligorsky MS, Am. J. Physiol. Physiol1999, 277, F882–F889.

[31]. Scapagnini G, D'Agata V, Calabrese V, Pascale A, Colombrita C, Alkon D, Cavallaro S, Brain Res. 2002, 954, 51–59. [PubMed: 12393232]

[32]. Piantadosi CA, Zhang J, Levin ED, Folz RJ, Schmechel DE, Exp. Neurol1997, 147, 103–114. [PubMed: 9294407]

[33]. Tang Y-P, Murata Y, Nagaya T, Noda Y, Seo H, Nabeshima T, Cereb J. Blood Flow Metab. 1997, 17, 771–780.

[34]. Zhuo M, Small SA, Kandel ER, Hawkins RD, Science (80-.). 1993, 260, 1946–1950.

[35]. Gee KR, Brown KA, Chen W-NU, Bishop-Stewart J, Gray D, Johnson I, Cell Calcium2000, 27, 97–106. [PubMed: 10756976]

[36]. Wilkinson WJ, Kemp PJ, J. Physiol2011, 589, 3055–3062. [PubMed: 21521759]

[37]. Peers C, Boyle JP, Scragg JL, Dallas ML, Al-Owais MM, Hettiarachichi NT, Elies J, Johnson E, Gamper N, Steele DS, Br. J. Pharmacol2015, 172, 1546–1556. [PubMed: 24818840]

[38]. Lim I, Gibbons SJ, Lyford GL, Miller SM, Strege PR, Sarr MG, Chatterjee S, Szurszewski JH, Shah VH, Farrugia G, Am. J. Physiol. Liver Physiol2005, 288, G7–G14.

[39]. Ambrósio AF, Silva AP, Malva JO, Soares-da-Silva P, Carvalho AP, Carvalho CM, Neuropharmacology1999, 38, 1349–1359. [PubMed: 10471089]

[40]. Canales A, Jia X, Froriep UP, Koppes RA, Tringides CM, Selvidge J, Lu C, Hou C, Wei L, Fink Y, Anikeeva P, Nat. Biotechnol2015, 33, 277. [PubMed: 25599177]

[41]. Matsuda S, Harada K, Ito M, Takizawa M, Wongso D, Tsuboi T, Kitaguchi T, ACS Sensors2017, 2, 46–51. [PubMed: 28722423]

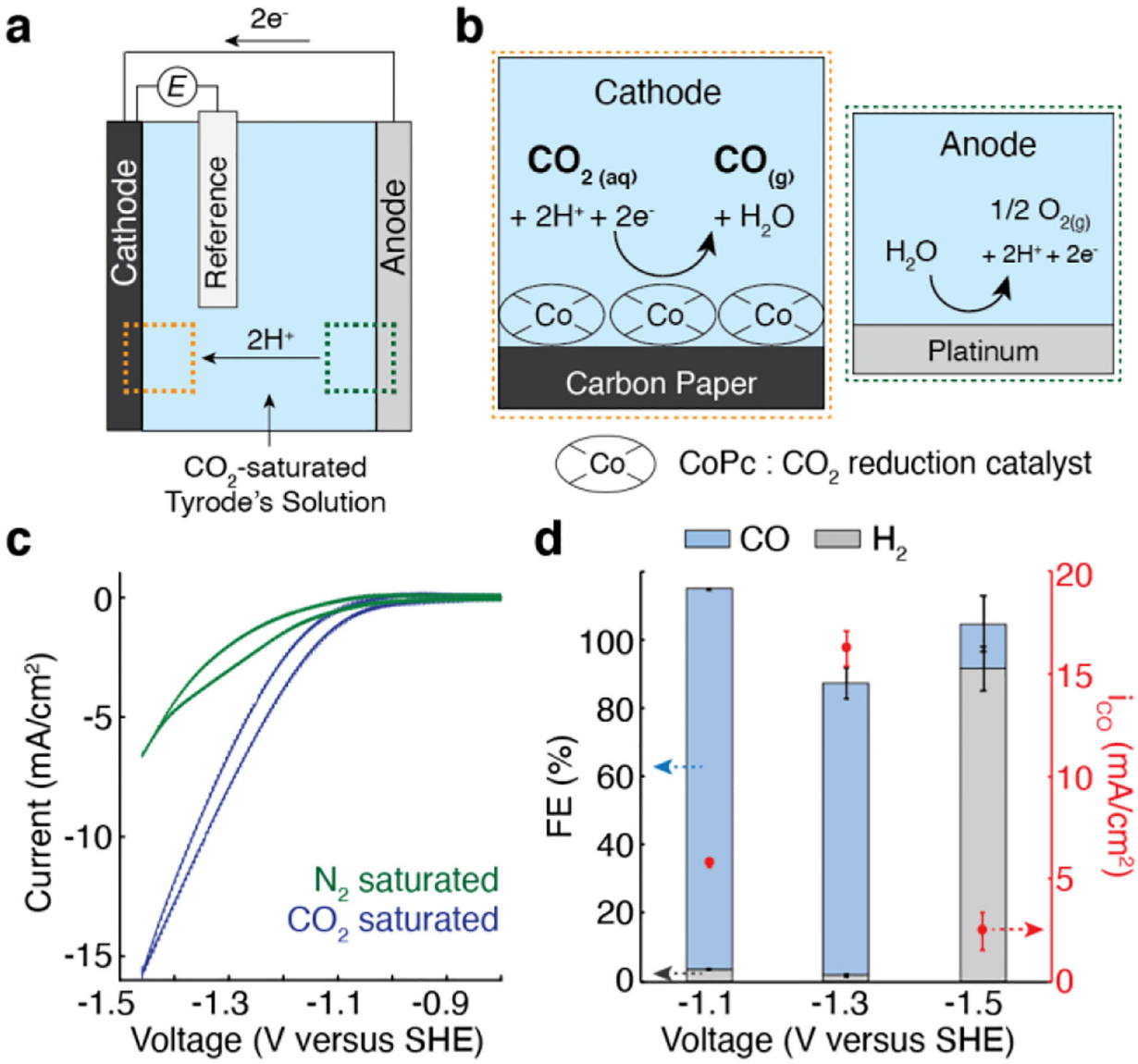

Figure 1.

a, A schematic illustrating the electrochemical system for in situ CO delivery. **b,** An illustration of the electrochemical reactions at the CoPc/OxCP cathode and Pt anode. **c,** CV curves of CoPc/OxCP electrodes in CO_2− (blue) or N_2− (green) saturated Tyrode's solution at pH 7.4 (scan rate, 100 mV/s). **d,** The Faradaic efficiency (FE) for CO and H_2, and partial current density of CO (i_{CO}) (mean ± standard error of the mean (s.e.m.), n = 3) at various applied voltages.

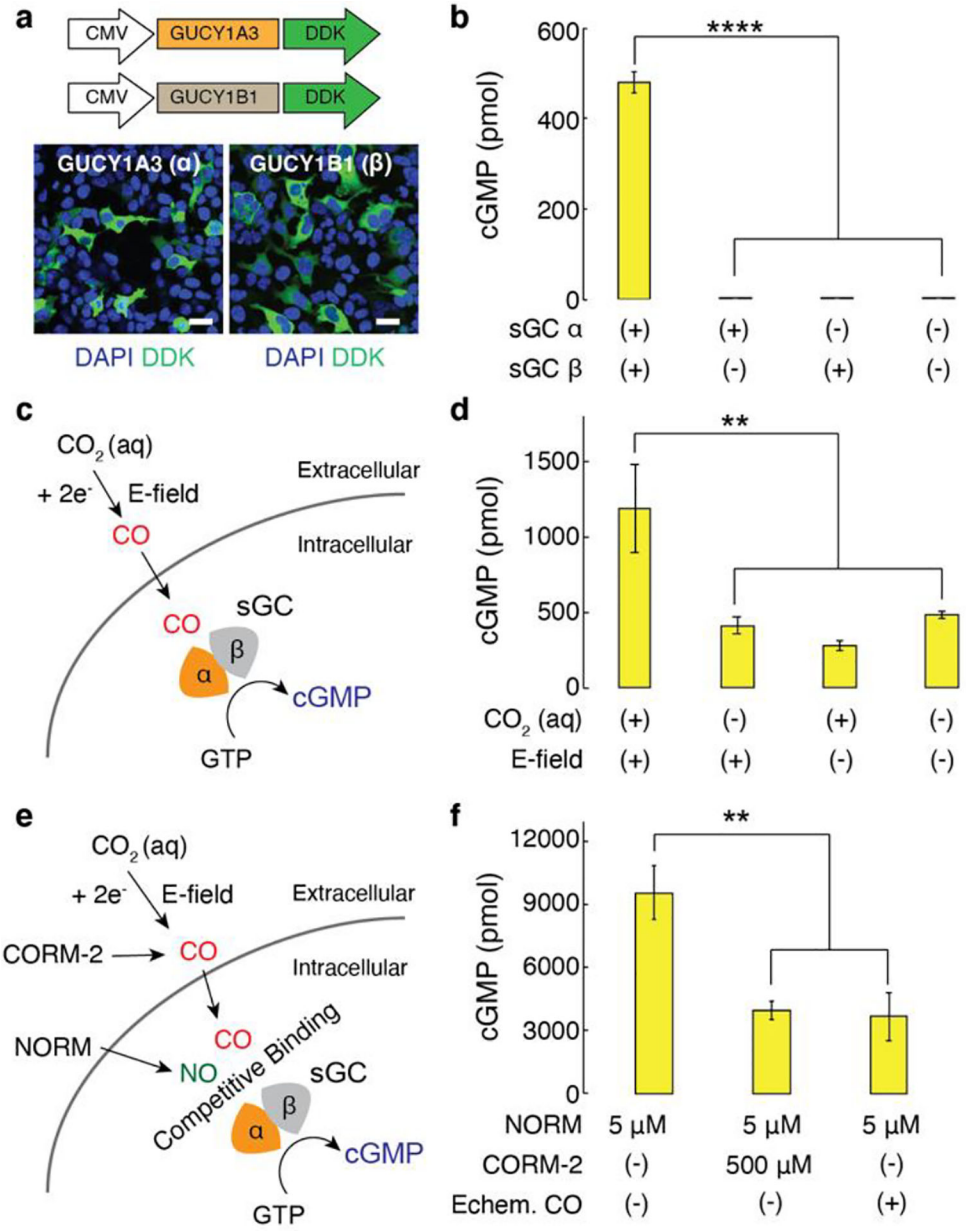

Figure 2.

a, Representative confocal images of HEK cells transfected with DDK-tagged α-subunit of sGC or DDK-tagged β-subunit of sGC under the CMV promoter (scale bar, 50 μm). **b,** Intracellular cGMP levels (mean ± s.e.m.) in 10^6 HEK cells 48 h after the transfection (n = 6, one-way analysis of variance (ANOVA) and Tukey's multiple comparison test, $F_{3,20} = 392.2$, **** $p = 1.1 \times 10^{-16} < 0.0001$). **c,** A schematic illustrating activation of sGC mediated by electrochemically produced CO. GTP, guanosine 5' triphosphate. **d,** Intracellular cGMP levels (mean ± s.e.m.) in 10^6 sGC^+ cells following CO delivery driven by CoPc/OxCP cathodes at −1.3 V versus SHE for 10 min. The statistical significance of an increase in cGMP levels after electrochemical CO delivery as compared with controls was assessed by one-way ANOVA and Tukey's multiple comparison test (n = 6, $F_{3,20} = 7.4$, **

$p = 0.0016 < 0.01$). **e,** An illustration of NO-sGC-cGMP signaling pathways modulated by CO. NORM, nitric oxide releasing molecule. **f,** Intracellular cGMP levels (mean ± s.e.m.) in 10^6 sGC^+ cells following NO delivery in the presence or absence of CO (n = 5, one-way ANOVA and Tukey's multiple comparison test, $F_{2,12} = 10.9$, ** $p = 0.002 < 0.01$).

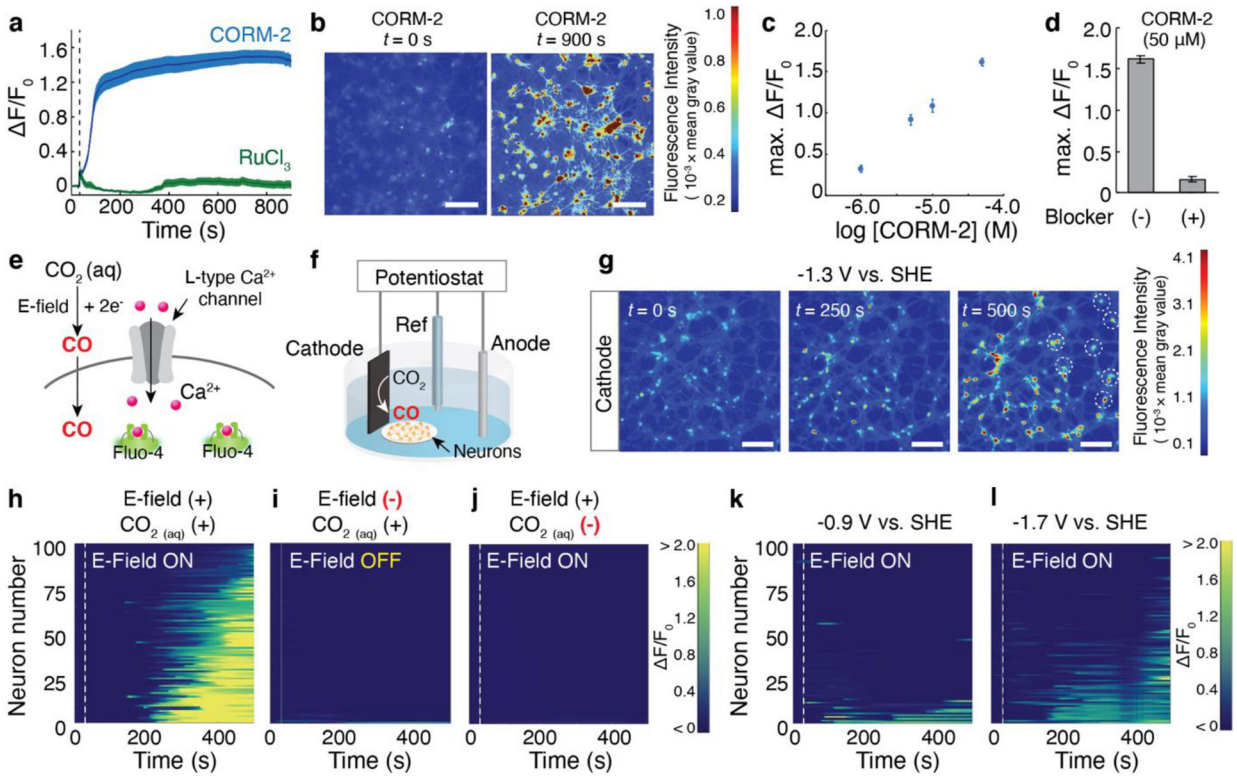

Figure 3.

a, Averaged fluo-4 fluorescence traces for hippocampal neurons (n = 100 neurons for each trace) following 50 μM CORM-2 (blue) or 50 μM $RuCl_3$ (green) infusion at 30 s (dashed lines). The solid lines and shaded areas represent the mean and s.e.m., respectively. **b,** Time-lapse images of Ca^{2+} responses in response to CORM-2 infusion (scale bar, 50 μm). **c,** CORM-2 concentration-dependent maximum of normalized fluo-4 fluorescence change averaged across 100 neurons. **d,** Maximum of normalized fluo-4 fluorescence increases in 100 neurons following the infusion of 50 μM CORM-2 in the presence or absence of L-type Ca^{2+} channel blocker nitrendipine. **e,** A schematic illustrating a potential mechanism of CO-mediated Ca^{2+} responses in neurons through L-type Ca^{2+} channel. **f,** Experimental scheme for electrochemical CO delivery to neurons. **g,** Time-lapse images of Ca^{2+} increases in neurons triggered by CO produced from CoPc/OxCP cathodes, which were positioned at the left edge in all three images, at −1.3 V versus SHE (scale bar, 50 μm). Neurons located at greater distances from the cathode responded over time (white dotted circles). **h-j**, Individual fluo-4 fluorescence traces for 100 neurons at different experimental conditions. E-field (–) in **(i)** represents neurons immersed in CO_2-saturated solution in the absence of an applied voltage. $CO_{2(aq)}$ (–) in **(j)** represents neurons immersed in Tyrode's not saturated in CO_2 in the presence of an applied voltage **(j)**. Voltage of −1.3 V were turned on at 30 s (dashed lines) in **h** and **j**. **k-l,** Individual fluo-4 fluorescence traces for 100 neurons after electrochemical CO generation at −0.9 V (**k**) and −1.7 V versus SHE (**l**). Voltages were turned on at 30 s (dashed lines).

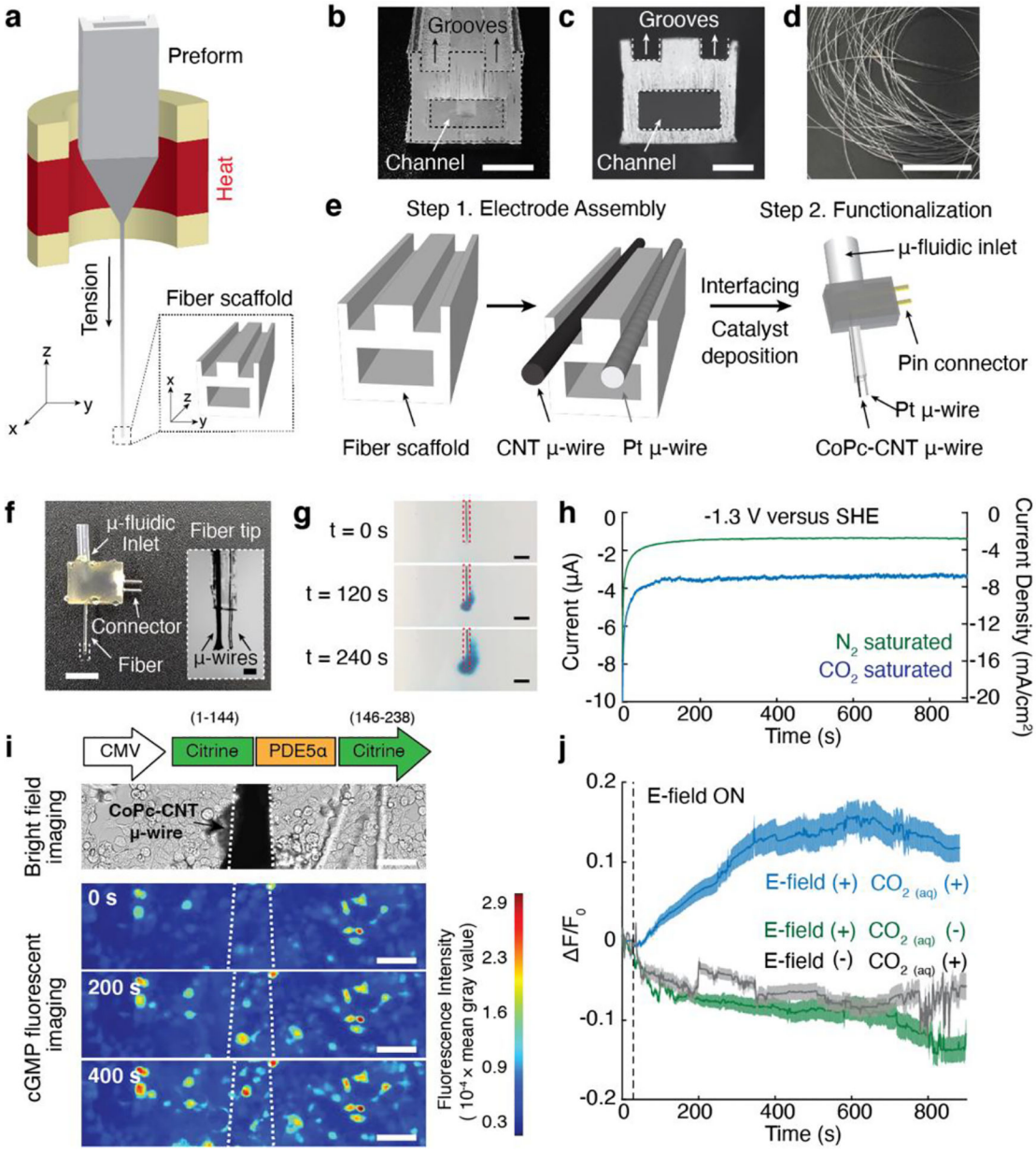

Figure 4.

a, A schematic illustrating the fiber drawing procedure. **b-c,** Cross-sectional images of the preform (**b**, scale bar, 5 mm) and the fiber scaffold after the drawing process (**c,** scale bar, 100 μm). Two microscale grooves and one hollow microchannel are visible in **c**. **d,** A photograph of a bundle of fiber scaffolds after the drawing process (scale bar, 5 cm). **e,** A schematic demonstrating microelectrode assembly on the fiber scaffold, followed by fiber connectorization and functionalization of the CNT microwires with CoPc catalyst. **f,** A photograph of the resulting CO delivery fiber (scale bar, 5 mm) and a microscope image of the fiber tip (inset, scale bar, 100 μm). **g,** Delivery of CO_2-saturated Tyrode's solution with a dye (BlueJuice) into a brain phantom (0.6% agarose gel) through the microfludic channel within the fiber at an infusion rate of 100 nL/min (scale bar, 500 μm).

h, Chronoamperometry measurements conducted with the electrocatalytic fiber in CO_2-saturated (blue) or N_2-saturated (green) Tyrode's solution at pH 7.4. **i,** An optical image of a CoPc-CNT microwire of the CO-delivery fiber positioned above Green cGull-expressing cells (top). Time-lapse images of local cGMP dynamics in Green cGull-expressing cells in response to electrochemically synthesized CO from the CoPc-CNT microwire (white dotted lines) at −1.3 V versus SHE (scale bar, 50 μm) (bottom). **j,** Averaged Green cGull fluorescence traces of cells (n = 100 cells for each trace) at different experimental conditions. The solid lines and shaded areas indicate the mean and s.e.m., respectively. E-field (–) and $CO_{2(aq)}$ (–) indicate cells after delivery of CO_2-saturated solution in the absence of an applied voltage and cells subjected to cathodic voltage without CO_2 saturation, respectively. Voltages of −1.3 V were turned on at 30 s (dashed lines).